processes

MDPI

Article

Investigations on Amoxicillin Removal from Aqueous Solutions by Novel Calcium-Rich Biochars: Adsorption Properties and Mechanisms Exploration

Salah Jellali [1,*], Wissem Hamdi [2], Majida Al-Harrasi [3], Malik Al-Wardy [1], Jamal Al-Sabahi [4], Hamed Al-Nadabi [1], Ahmed Al-Raeesi [1] and Mejdi Jeguirim [5]

[1] Centre for Environmental Studies and Research, Sultan Qaboos University, Al-Khoud, Muscat 123, Oman; hamed@squ.edu.om (H.A.-N.); aalraeesi@squ.edu.om (A.A.-R.)
[2] Higher Institute of the Sciences and Techniques of Waters, University of Gabes, Gabes 6029, Tunisia; wissemhemdi@yahoo.fr
[3] Department of Plant Sciences, College of Agricultural and Marine Sciences, Sultan Qaboos University, Al-Khoud, Muscat 123, Oman; mageda502@gmail.com
[4] Central Instrumentation Laboratory, College of Agricultural and Marine Sciences, Sultan Qaboos University, Al-Khoud, Muscat 123, Oman; jamal@squ.edu.om
[5] The Institute of Materials Science of Mulhouse (IS2M), University of Haute Alsace, University of Strasbourg, CNRS, UMR 7361, F-68100 Mulhouse, France; mejdi.jeguirim@uha.fr
* Correspondence: author: s.jelali@squ.edu.om

Abstract: This study investigates the synthesis, characterization, and environmental application for amoxicillin (AMX) removal in batch mode of three novel calcium-rich biochars. These biochars were produced from the co-pyrolysis of poultry manure, date palm wastes, and waste marble powder at temperatures of 700 °C (Ca-B-700), 800 °C (Ca-B-800), and 900 °C (Ca-B-900). Characterization results show that increasing the pyrolysis temperature results in improved structural, textural, and surface chemistry properties. For instance, the BET surface area of the Ca-B-900 was assessed to be 52.3 m^2 g^{-1}, which is 14.1 and 3.1 times higher than those observed for Ca-B-700 and Ca-B-800, respectively. Moreover, the Ca-B-900 shows higher AMX removal ability (56.2 mg g^{-1}) than Ca-B-800 (46.8 mg g^{-1}), Ca-B-700 (14.6 mg g^{-1}), and numerous other engineered biochars. The AMX removal process by these biochars is favorable under wide experimental conditions of initial pH and AMX concentrations. Additionally, the experimental and modeling data show that the AMX adsorption process includes both physical and chemical mechanisms. This study confirms that Ca-rich biochars can perform significant removal of AMX in batch mode.

Keywords: wastes management; engineered biochars; pharmaceuticals removal; adsorption characteristics; mechanism

Citation: Jellali, S.; Hamdi, W.; Al-Harrasi, M.; Al-Wardy, M.; Al-Sabahi, J.; Al-Nadabi, H.; Al-Raeesi, A.; Jeguirim, M. Investigations on Amoxicillin Removal from Aqueous Solutions by Novel Calcium-Rich Biochars: Adsorption Properties and Mechanisms Exploration. *Processes* **2024**, *12*, 1552. https://doi.org/10.3390/pr12081552

Academic Editors: Dimitris Zagklis and Georgios Bampos

Received: 4 July 2024
Revised: 23 July 2024
Accepted: 24 July 2024
Published: 25 July 2024

1. Introduction

Studies on emerging contaminants have attracted significant attention over the last two decades [1]. These substances, including herbicides, pesticides, micro- and nano-plastics, new organic dyes, and pharmaceuticals, have been increasingly detected in water ecosystems [2]. Even at very low concentrations, these compounds may have serious adverse impacts on both aquatic systems and also human health [3]. Special attention has been given to the pharmaceutical compounds due to their significant usage and the rising concentrations detected in water resources [4]. This presence is attributed to uncontrolled discharges from the pharmaceutical industry and the excretion of these substances in urine and feces by humans in hospitals and animals on farms [5]. Active pharmaceutical substances are highly resistant to biodegradation and thus persist in aquatic ecosystems. This persistence can adversely affect aquatic organisms and subsequently affect human health through the food chain [4]. Amoxicillin is an active compound that belongs to the

penicillin family. It is one of the most widely used antibiotics in the majority of European countries [6]. Moreover, around 80% of the orally ingested AMX is excreted into the urine in a non-metabolized form and consequently transferred to wastewater treatment plants [7].

Numerous technologies have been tested for the removal of pharmaceuticals from aquatic environments. They mainly include membrane advanced oxidation processes, membrane filtration, and biological degradation [8]. However, the real application of these methods can be challenging due to the required stringent experimental conditions, high energy consumption, and the possible production of toxic by-products [9]. Adsorption methods have been pointed out as an attractive and promising approach for removing pharmaceuticals due to their simple design and operation, minimal energy requirements, eco-friendliness, and high effectiveness [10]. Numerous materials, such as raw agricultural wastes [11], activated carbons [12], molecular organic frameworks [13], and biochars [10] have been applied to purify water from pharmaceuticals. However, biochar constitutes a more cost-effective option for the elimination of pharmaceutical residues, valued by its environmental benefits and sustainability, low cost, and adaptability for large-scale use [14,15]. For instance, on the environmental side, the production of 1 kg of biochar requires only 6.1 MJ and has net negative greenhouse gas emissions (−0.9 kg CO_2 eq). These values are much more attractive when compared to those corresponding to the generation of 1 kg of activated carbon: 97 MJ and + 6.6 kg CO_2 eq [9].

Calcium-rich biochars are novel materials that are typically synthesized from the pyrolysis of pre-impregnated biomasses or post-impregnated biochars with calcium chloride chemical reagents ($CaCl_2$) [16,17]. In this last decade, to reduce the use of chemicals and to boost sustainability and circular economy concepts, various Ca-rich biochars were produced from the co-pyrolysis of biomasses mixed with calcium-based wastes such as powder marble [18], oyster shell [19], crab shells [20], eggshell [21], and dolomite [22]. The characteristics of the synthesized biochars depend mainly on the percentage of the mineral waste and also the pyrolysis conditions [23–25]. Usually, improved textural properties (i.e., surface area and porosity) are obtained when increasing the pyrolysis temperature and the pyrolysis contact time or decreasing the percentage of the Ca-based wastes [25–28]. For instance, Wang et al. [24] showed that increasing the corn straw/eggshell mass ratio from 1:0 to 1:4 and 2:3 decreased the BET surface area of the related biochars from 179.7 to 67.5 and only 23.6 $m^2\ g^{-1}$, respectively. Moreover, Xu et al. [19] showed that increasing the pyrolysis temperature from 700 to 900 °C of a mixture of rice husk and oyster shells (at a mass ratio of 1:2) increased the BET surface area and the total pore volume from 21.3 $m^2\ g^{-1}$ and 0.025 $cm^3\ g^{-1}$ to 46.2 $m^2\ g^{-1}$ and 0.019 $cm^3\ g^{-1}$, respectively. A similar trend was observed for $Ca(OH)_2$-modified wood biochar [29].

In addition, most of the previous valorization studies of Ca-rich biochars for wastewater treatment have been concerned with nutrient recovery from wastewater (i.e., phosphorus (P)) [17,30]. In this regard, these biochars were found to be excellent materials for P recovery, even under challenging conditions [16]. However, only rare studies have investigated the use of Ca-rich biochars, which are synthesized from the co-pyrolysis of biomasses with Ca-based industrial wastes, for pharmaceuticals removal from aqueous solutions [29,31]. For instance, in the study of Zen and Kan [29], tetracycline removal by $Ca(OH)_2$-modified wood biochar was found to be moderately removed in batch mode (20.9 mg g^{-1}) and not removed in column mode. To the best of our knowledge, the only preliminary study regarding the use of Ca-rich biochar for AMX removal was recently carried out by our research work [31]. In this study, we synthesized a novel biochar at 900 °C from two abundant organic feedstocks and a mineral industrial waste: (i) an animal organic waste: poultry manure (PM), (ii) lignocellulosic biomass: date palm waste (DPW), and (iii) a Ca-based industrial waste: marble powder (WMP). Results of this study showed that this Ca-rich biochar (Ca-B-900) selectively recovered P, and no significant AMX removal was observed under dynamic conditions (both column and reactors). While this study provides valuable insights into the general behavior of AMX removal by Ca-B-900 in batch mode, a detailed and comprehensive understanding of the effect of pyrolysis temperature

as well as the adsorption experimental conditions (i.e., contact time, initial pH, initial AMX concentration, etc.) on AMX removal efficacy is still lacking. Moreover, the involved mechanisms in this pharmaceutical removal by Ca-rich biochars were not yet appropriately illustrated [29,31]. Further investigations are needed in order to overcome this knowledge gap and also to facilitate the future upscaling process for real-site conditions application.

Therefore, the present research work aims to (i) synthesize Ca-rich biochars from the co-pyrolysis of poultry manure, date palm waste, and waste marble powder at three different temperatures: 700, 800, and 900 °C, (ii) characterize these biochars by using various analytical methods, (iii) study the AMX removal efficiency in batch mode and under different experimental situations encompassing contact time, initial pH, adsorbent dosage, ionic strength, and initial AMX concentration, and (iv) explore the main involved mechanisms in this removal process.

2. Materials and Methods

2.1. Feedstock Preparation and Biochars Synthesis

Three feedstocks were used during this work: PM, DPW, and WMP. The PM and dry DPW were provided from a local farm in Muscat, Oman. They were air-dried until they reached a nearly constant weight, then ground using a mechanical grinder and sieved. The fraction with a dimension lower than 1 mm was selected and used hereafter for the production of the biochars. The WMP was collected from an industrial site in Oman in a slurry form. It was air-dried until a constant weight and used without any modification. A feedstock mass of 100 g was prepared by a manual mixing of 45 g of PM, 10 g of DPW, and 45 g of WMP, respectively, and used for the production of the biochars. The chosen WMP percentage should permit the formation of enough contents of CaO and $Ca(OH)_2$. It is in line with previous works [21,32].

The Ca-rich biochars synthesis was performed using an electric tubular furnace (Carbolite, TF1-1200, Neuhausen, Germany) under an N_2 atmosphere. The heating gradient and residence time were kept constant at 5 °C min^{-1} and 2 h, respectively. Three biochars were synthesized at final pyrolysis temperatures of 700, 800, and 900 °C. They were labelled Ca-B-700, Ca-B-800, and Ca-B-900, respectively. These pyrolysis temperatures were chosen in order to elucidate the effect of WMP carbonization degree and the biochars' calcium oxide contents on AMX removal efficiency. They are in line with previous studies [18,19]. These biochars were kept in plastic airtight containers and used for AMX removal assays from aqueous solutions. The biochars production yields at a given temperature pyrolysis 'T' (Y_T (%)) were calculated as follows:

$$Y_T\ (\%) = \frac{M_{f,T}}{M_{0,T}} \times 100 \quad (1)$$

where $M_{0,T}$ and $M_{f,T}$ are the feedstock mixture masses before and after the pyrolysis process at a fixed pyrolysis temperature.

2.2. Biochars Characterization

During this work, the three synthesized biochars were characterized through the analysis of their (i) surface morphology and elemental composition by a scanning electron microscope (SEM) coupled with energy dispersive X-ray (EDS) (Jeol, Jsm-7800F, Tokyo, Japan), (ii) mineral composition by X-ray fluorescence device (XRF) (Rigaku, Nexqc, Tokyo, Japan), (iii) crystallinity through X-ray diffraction (XRD) (Rigaku, Miniflex 600, Tokyo, Japan), (iv) pores properties (BET surface areas, total pore volumes (TPV), and average pore sizes (APS) by a Micrometrics instrument (ASAP-2020, Ottawa, ON, Canada), (v) functional groups richness by Fourier Transform Infrared (FTIR) (Perkin Elmer, Frontier, MA, USA), and (vi) the surface charge versus pH on the basis of the pH drift method [33].

2.3. Amoxicillin Adsorption Experiments

2.3.1. Chemicals

The AMX reagent used in this work (chemical formula: $C_{16}H_{19}N_3O_5S$; molecular weight: 365.4 g mol^{-1}) was purchased from Sigma-Aldrich, St. Louis, MO, USA. It was employed for the preparation of a stock solution of 1000 mg L^{-1}, which has been used throughout this study. This solution was diluted by using distilled water to obtain the desired synthetic solution concentrations. Moreover, NaOH and HCl (from Sigma-Aldrich) were used for the adjustment of the prepared solutions' pH values. These values were measured by a dedicated pH meter (Mettler Toledo, Columbus, OH, USA).

2.3.2. Batch Assays Experimental Protocol and Data Analysis

The efficiency of the three Ca-rich biochars in removing AMX from aqueous solutions was performed under static conditions (batch mode). This step was ensured through controlled shaking adsorbent within AMX solutions in 120 mL glass flasks by a multi-position magnetic stirrer (Gallenkamp, Cambridge, UK) at 600 rpm. The biochars' effectiveness in removing AMX was assessed through sample analyses before and after adsorption. These samples were first filtrated through 0.22 µm PVDF filters (Whatman, Buckinghamshire, UK) and then analyzed by high-performance liquid chromatography (HPLC, Shimadzu, Kyoto, Japan). The effect of various parameters (i.e., contact time, initial pH, biochar dosage, and initial concentration) on AMX removal by the three biochars was studied under the conditions given in Table 1. The interval variation of these parameters was fixed on the basis of our previous study [34] and also preliminary investigations.

Table 1. Experimental conditions used for AMX removal by the Ca-rich biochars.

Experimental Set	Contact Time (h)	pH	Biochar Dosage (g L^{-1})	Dissolved NaCl/Na_2SO_4 (mM L^{-1})	Initial Concentration (mg L^{-1})
Effect of contact time	From 1 min to 24 h	6.8	1	0/0	100
Effect of pH	24	4–10	1	0/0	100
Effect of dose	24	6.8	0.1–40	0/0	100
Effect of ionic strength	24	6.8	1	14–42/0	100
	24	6.8	1	1–5.2/0	100
Effect of initial concentration	24	6.8	1	0/0	5–100

The adsorbed AMX amount after a desired contact time 't' (q_t), and the corresponding removal yield (R_t) were assessed as follows:

$$q_t = \frac{(C_0 - C_t) * V}{Mb} \quad (2)$$

$$R_t(\%) = \frac{(C_0 - Ct)}{C_0} \times 100 \quad (3)$$

where C_0 and C_t (mg L^{-1}) are the AMX concentrations before adsorption and after a contact time of 't', respectively. Mb and V are the mass of the biochar (g) and the volume of the solutions (L), respectively.

To obtain a better understanding of the AMX kinetic adsorption process by the three biochars, the related experimental data were fitted to three famous models, namely pseudo-first-order (PFO), pseudo-second-order (PSO), and diffusion models (WM). Similarly, Freundlich, Langmuir, and Dubinin-Radushkevich (D-R) models were used to fit the experimental isotherm data. The equations of these kinetic and isotherm models, as well as the definition of the included parameters, are provided in the Supplementary Materials

(Table S1). The agreement between the experimental and these models-calculated curves was assessed by estimating the related correlation coefficients (R^2) as well as the mean absolute percentage errors (MPAE) as follows:

$$MAPE_{kinetic} = \frac{\sum \left| \frac{q_{t,\exp} - q_{t,pred}}{q_{t,\exp}} \right|}{N} * 100 \quad (4)$$

$$MAPE_{isotherm} = \frac{\sum \left| \frac{q_{e,\exp} - q_{e,pred}}{q_{e,\exp}} \right|}{N} * 100 \quad (5)$$

where $MAPE_{kinetic}$ and $MAPE_{isotherm}$ are the mean absolute percentage errors between the experimental and predicted kinetic and isotherm data, respectively. The $q_{t,exp}$, $q_{t,pred}$ and $q_{e,exp}$ and $q_{e,pred}$ denote the experimental and predicted adsorbed AMX quantity at time 't' and at equilibrium, respectively. N represents the number of experimental runs.

All the cited above batch experimental data were carried out at least in triplicate. The experimental results given in this work represent the average values.

2.3.3. Statistical Analysis

Excel 2016 was used for figure plotting and the regression analysis of the experimental and predicted data. The error bars in the plots are the standard deviation that is estimated from the triplicate batch assays.

3. Results

3.1. Biochars Characterization

The biochar production yields were assessed to be 63.9%, 57.5%, and 42.6% for Ca-B-700, Ca-B-800, and Ca-B-900, respectively (Table 2). The decrease of this yield production with the increase of the temperature is expected and is imputed to a higher decomposition rate of the volatile matter contained in the used feedstocks [35]. It is important to mention that these yields are much higher than those usually reported for lignocellulosic, animal, or even sludge biomasses [35–37]. This is mainly due to the mineral nature of the WMP, which is only slightly carbonized even at high pyrolysis temperatures [38,39].

Table 2. Main properties of the three synthesized calcium-rich biochars (BET SA: Brunauer–Emmett–Teller Surface area; TPV: total pore volume, APS: average pore size).

Biochar	Yield (%)	Mineral Contents (mg g^{-1})									Textural Properties			pHzpc
		Ca	K	P	Fe	Mn	Ni	Zn	Cu	Cd	BET SA (m^2 g^{-1})	TPV (cm^3 g^{-1})	APS (nm)	
Ca-B-700	63.9	219.0	10.8	9.4	0.76	0.25	0.18	0.15	0.04	0.01	3.7	0.013	35.1	10.89
Ca-B-800	57.5	245.0	11.4	9.4	0.87	0.26	0.19	0.16	0.05	0.01	16.9	0.018	15.1	13.30
Ca-B-900 [31]	42.6	324.0	12.3	12.4	1.03	0.34	0.22	0.12	0.06	0.08	52.3	0.032	9.4	13.46

The SEM images of the Ca-B-700, Ca-B-800, and Ca-B-900 are given in Figure S1. It can be clearly seen that the three biochars present irregular surfaces and a sponge-like structure containing pores with different dimensions. The Ca-B-900 seems to have a better structure with finer aggregates due to the fact that higher pyrolysis temperatures induce more volatilization of organic matter present in the mixed organic feedstocks and also a larger transformation yield of waste marble powder into calcium oxides/hydroxides [40,41]. The latter assumption is in line with the semi-qualitative EDS analyses, which indicate that the Ca peaks increase with the rise of the pyrolysis temperature (Figure S1). Additionally, the XRD analyses (Figure 1a–c) clearly show that at 700 °C, no significant transformation of $CaCO_3$ was observed (Figure 1a). However, as the pyrolysis temperature increases, the $CaCO_3$ transformation into CaO and $Ca(OH)_2$ is favored (Figure 1b–c). The highest

transformation rate was observed at a temperature of 900 °C, where more Ca-based oxide contents were observed (Figure 1c). At this temperature, non-negligible peaks of CaO; and $Ca(OH)_2$ are detected at 2θ of 32.4°, 37.5°, 54.2°, 64.3°, and 67.5°; and at 18.1°, 28.4°, 28.8°, 34.2°, 51.0°, 62.5°, and 64.3°, respectively. This result is in concordance with that of [38], who studied the pyrolysis of marble originating from Turkey. They showed that its carbonization process occurs between around 650 and 850 °C with a maximum mass loss of 41.3% at 1000 °C. Moreover, Ca-based nanoparticles ($CaO/Ca(OH)_2$) detection was reported for Ca-rich biochars generated from the co-pyrolysis of eggshells mixed with corn straw [21] or with peanut shells [42], and oyster shells mixed with peanut shells [43] or ground coffee waste [32]. A similar finding was also reported for Ca-rich biochar generated from the pyrolysis of pure crab shells [26].

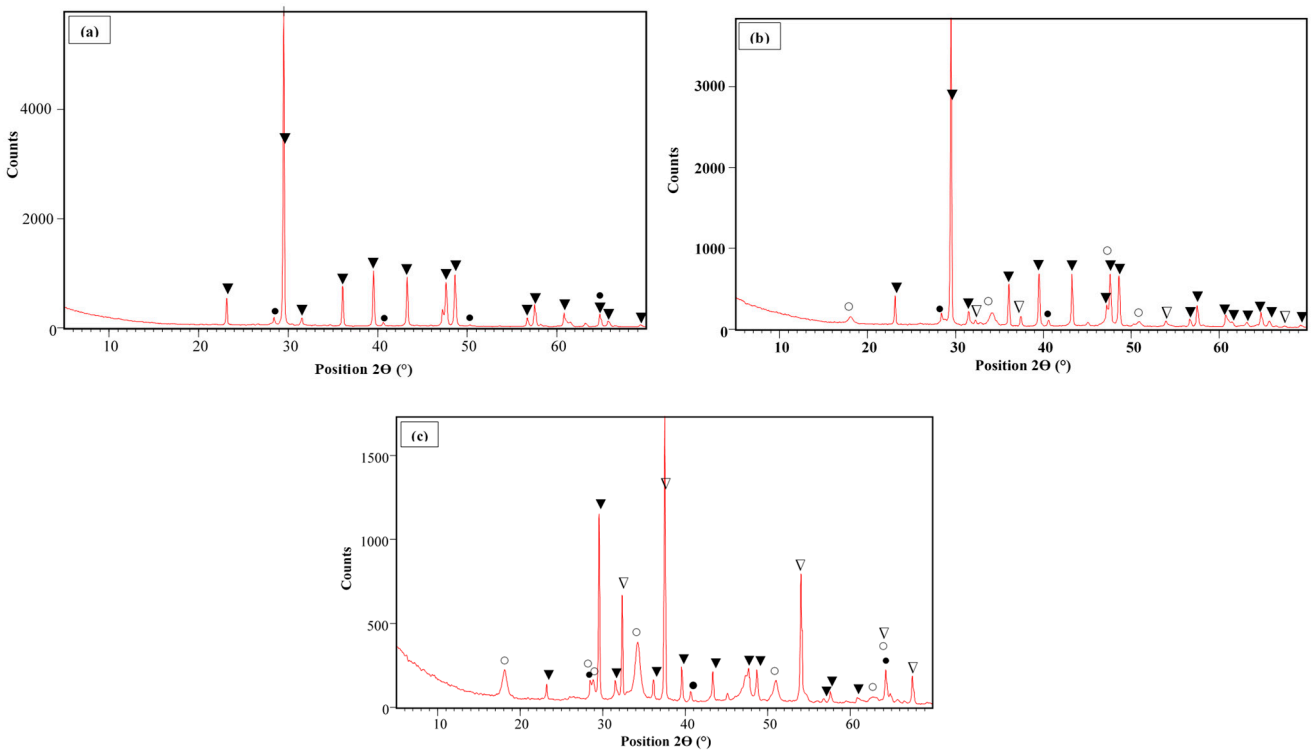

Figure 1. XRD analyses of Ca-B-700 (**a**), Ca-B-800 (**b**), and Ca-B-900 (**c**) [31] (▲: $CaCO_3$; ●: KCl; Δ: CaO; ○: $Ca(OH)_2$).

The WMP carbonization and conversion into Ca-based oxides are further confirmed by the XRF analyses (Table 2). Indeed, the Ca contents increased from 219 mg g^{-1} for Ca-B-700 by 11.9% and 47.9% for Ca-B-800 and Ca-B-900 [31], respectively. These Ca contents increases are due to the higher volatilization rate of the organic matter contained in the PM and DPW feedstocks and also the better calcination of the WMP. The same increase trend was observed for the majority of the minerals such as P, K, Fe, Mn, etc. (Table 2). For instance, the potassium content observed at 700 °C has increased by around 5.6% and 13.9% in Ca-B-800 and Ca-B-900 [31], respectively. Moreover, most of the toxic heavy metals in the three synthesized biochars have relatively low contents (Table 2). Other heavy metals presented contents lower than the detection limit of the used ICP/MS apparatus: As, Al, Hg, and Co.

In addition, the textural properties of the synthesized biochars were significantly improved with the increase of the pyrolysis temperature (Table 2 and Figure 2). Indeed, compared to Ca-B-700, the BET surface areas and 'TPV' of Ca-B-800 and Ca-B-900 have increased by 356.8% and 1313.5%, and '38.5%' and '146.2%', respectively. This indicates that the deposition of Ca-based nanoparticles on the biochars' surface did not contribute to the clogging of the biochars' pores. This can be explained by the fact that all the biochars

have mesoporous structures with average pore sizes varying in the range of 2 and 50 nm (Table 2). However, it is clear that the biochars' average pore sizes have decreased with the increase in temperature, tending to be microporous (Table 2). A comparable trend was observed for biochars derived from the co-pyrolysis of commercial wood biochar and $Ca(OH)_2$ at 100 and 300 °C [29]. However, some other studies have underlined that at high pyrolysis temperatures, biochars' structure may collapse, which can result in a significant decrease in the BET surface areas and the total pore volumes [44,45]. The enhanced textural properties of our Ca-rich biochars, especially Ca-B-900, may contribute to better AMX removal through physical adsorption processes [46].

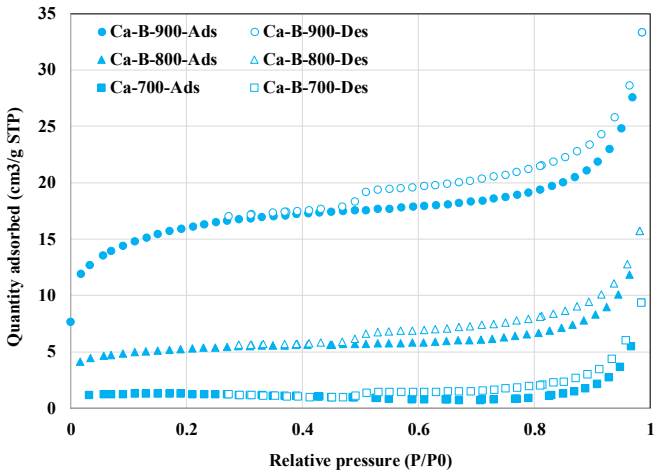

Figure 2. N_2 adsorption and desorption isotherms of the three synthesized Ca-rich biochars.

Finally, the pyrolysis temperature has an important effect on the surface chemistry of the synthesized biochars. Indeed, the FTIR spectra of these biochars (Figure 3) showed that they contain various functional groups such as hydroxyl, ketones, and carboxylic [26,40,45]. Furthermore, for all the synthesized biochars, Ca–O functional groups were observed at wavenumbers of 712, 875, and 2510 cm^{-1} [40,47]. This confirms the synthesized biochars richness in calcium that was observed in XRD (Figure 1) and XRF analyses (Table 2). Moreover, a narrow and strong peak of –OH groups was observed for Ca-B-800 and Ca-B-900 at 3643 cm^{-1} [31] (Figure 3) [48,49]. This observation confirms the XRD results, which indicated that $Ca(OH)_2$ nanoparticle formation was detected for only Ca-B-800 and Ca-B-900 [31] (see Figure 1). Such a peak was reported for Ca-rich biochars produced at 800 °C from the co-pyrolysis of bagasse waste mixed with marble powder [40] and also peanut shells mixed with oyster shells at 800 °C [43]. Finally, FTIR analyses showed the presence of P–O peaks at 566 and 1047 cm^{-1} [18], which confirms the high P contents (9.4–12.4 mg g^{-1}) observed with XRF analyses (see Table 2). The functional groups richness of the three synthesized biochars may favor the AMX adsorption through a complexation mechanism [50].

Moreover, the values of the pHzpc were evaluated to 10.89, 13.30, and 13.46 for Ca-B-700, Ca-B-800, and Ca-B-900 [31], respectively. The relatively high values observed at temperatures of 800 and 900 °C confirm the high transformation rates of WMP into CaO and $Ca(OH)_2$ that were pointed out by the XRD analyses. This indicates that the synthesized biochars surface will be positively charged for a large aqueous pH interval (lower than the corresponding pHzpc) and may retain negatively charged pollutants (i.e., AMX) through electrostatic interactions [50]. High alkaline pH values (11.9–12.0) were reported for $Ca(OH)_2$-modified biochars produced at temperatures varying between 100 and 500 °C [29].

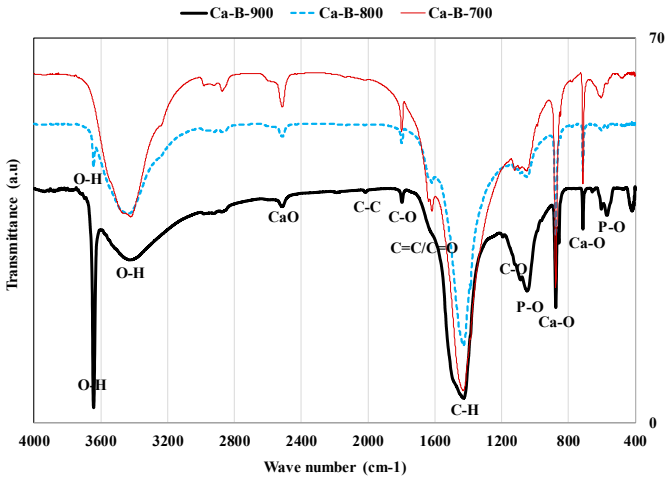

Figure 3. FTIR analyses of the three synthesized Ca-rich biochars.

3.2. Batch Adsorption Study

3.2.1. Impact of Contact Time—Kinetic Study

The AMX removal efficiency by the three synthesized Ca-rich biochars (Figure 4) shows that it is highly dependent on the contact time. Indeed, three kinetic phases can be distinguished. A first phase, where the kinetic rate is relatively rapid (until 8 h), followed by a slower one (until 20 h), then an equilibrium phase (between 20 and 24 h), where the AMX removed amounts remain quasi-constants. These three phases correspond to [34,51]: (i) diffusion through the boundary layer around the biochars particles, (ii) intraparticle diffusion where AMX is removed inside the mesoporous structure of the biochars, and (iii) the active sites of the biochars are saturated with AMX and no further adsorption is possible. For all biochars, the first phase seems to be the limiting step in the overall process because, for all the synthesized biochars, the corresponding diffusion coefficients (D_f) are lower than those of the intraparticle diffusion (D_{ip}) (Table 3). Similar findings were reported in previous studies related to pharmaceuticals removal by sludge-derived biochars [34,52]. The time required to reach the equilibrium state is evaluated to be around 20 h which is equivalent to those reported for sludge-derived biochars post-treated with Al, Fe, or Mn [53]. However, this time is higher than those reported for biochars generated from the pyrolysis of modified lignocellulosic biomasses such as a KOH-pretreated-cellulose fibers rejects (2 h) [54], a Zn-pretreated ginger waste (5 h) [46], and a Zn-pretreated corn cob (5–6 h) [51]. It is worth mentioning that the use of long contact times is not recommended in real applications due to the related high energetic expenses (i.e., pumping). In our case, a contact time of only 8 h can be suggested since it permits a relatively high removal percentage (Figure 4). Moreover, the PSO model fits better the experimental data for both Ca-B-800 and Ca-B-900 with rate constants of 2.2×10^{-4} and 4.6×10^{-4} g mg^{-1} min^{-1}, respectively (Table 3). Indeed, this model presents higher correlation coefficients and lower MAPE between the experimental and theoretical kinetic curves (Table 3). This suggests that the AMX removal process by these two biochars may involve chemical processes [53]. A similar finding was reported for AMX removal by biochars derived from sewage sludge [53] and from corn cobs [51]. The Ca-B-700 kinetic experimental data were better fitted with the PFO model, suggesting that the adsorption rate is mainly controlled by the diffusion process [55]. Additionally, the Ca-B-900 exhibits higher AMX removal efficiency in comparison with Ca-B-800 and Ca-B-700 (Figure 4). This is mainly attributed to its improved physico-chemical properties [29].

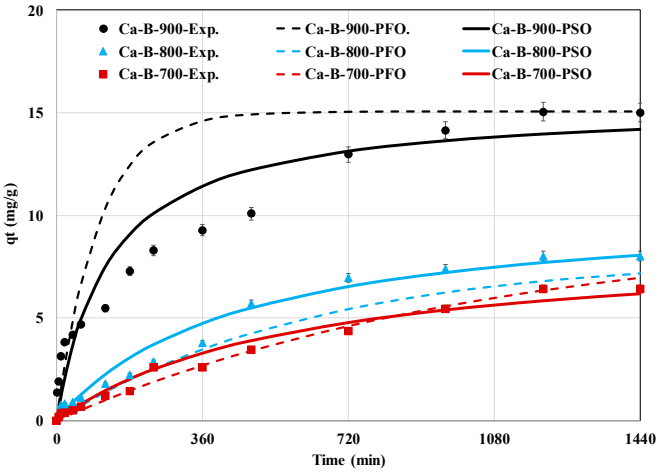

Figure 4. Experimental and predicted kinetic data of AMX removal by the synthesized calcium-rich biochars at 700, 800, and 900 °C.

Table 3. Parameters of the PFO and PSO kinetic models used for the AMX removal by Ca-rich biochars produced at 700, 800, and 900 °C.

	Parameter	Ca-B-700	Ca-B-800	Ca-B-900
PFO model	$q_{e,exp}$ (mg g^{-1})	6.4	8.0	15.1
	k_1 (min^{-1})	0.0009	0.0016	0.0096
	R^2	0.991	0.989	0.813
	MAPE (%)	18.0	26.7	43.1
PSO model	k_2 (g mg^{-1} min^{-1})	0.00019	0.00022	0.00046
	$q_{e,pred}$ (mg g^{-1})	8.8	10.5	15.9
	R^2	0.978	0.975	0.928
	MAPE (%)	21.7	20.5	28.9
Diffusion model	D_f ($\times 10^{-13}$ m^2 s^{-1})	0.39	0.52	1.45
	R^2	0.948	0.931	0.960
	D_{ip} ($\times 10^{-13}$ m^2 s^{-1})	1.56	1.87	1.57
	R^2	0.957	0.990	0.960

3.2.2. Impact of pH

The effect of pH on AMX removal by the three synthesized biochars was investigated for pH values varying between 4 and 10 while maintaining the contact time, the initial concentration, and the adsorbent dosage constants at 24 h, 100 mg L^{-1}, and 1 g L^{-1}, respectively. This wide pH interval was chosen because the electrical properties of both the adsorbent and the AMX are dependent on the aqueous pH values. Indeed, the AMX has three pKa values depending on its three possible ionizable forms [56]: carboxylic acid (pKa_1 = 2.7), primary amine group (pKa_2 = 7.5), and hydroxyl group (pKa_3 = 9.63). AMX is positively charged, zwitterionic (exists in two ionic forms AMX±), and negatively charged for pH values lower than pKa_1, between pKa_1 and pKa_2, and higher than pKa_3, respectively. Regarding our synthesized biochars, the Ca-B-700, Ca-B-800, and Ca-B-900 have pHzpc values of 10.89, 13.30, and 13.46 (see Table 2), indicating that for the studied pH range, their surface will be positively charged. Therefore, the adsorption of the negatively charged forms of AMX (observed for pH values higher than pKa1) will be well favored across the whole pH range studied through electrostatic interactions. In our case, for all the biochars, the AMX adsorbed amounts were almost constant for the tested pH range (Figure 5). The average AMX removed masses were quantified to 6.6, 8.4, and 15.3 mg g^{-1} for Ca-B-700,

Ca-B-800, and Ca-B-900, respectively. Relatively similar behavior was observed for AMX removal by a biochar derived from palm oil bunch waste [57].

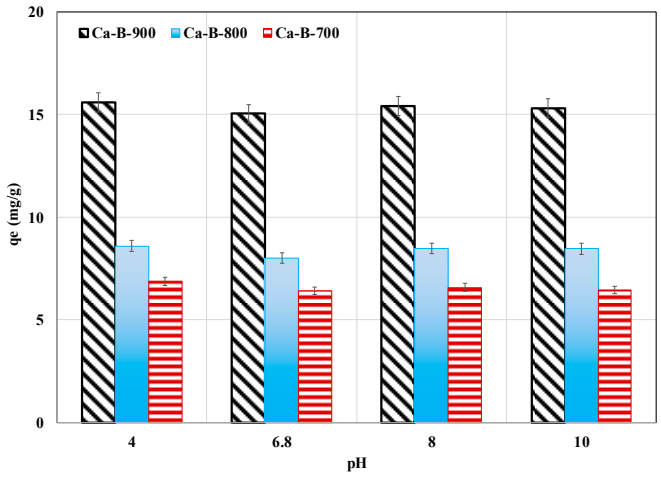

Figure 5. pH effect on AMX removal by Ca-B-700, Ca-B-800, and Ca-B-900.

3.2.3. Impact of Adsorbent Dose

The impact of the synthesized Ca-rich biochars in removing AMX from aqueous solutions was carried out for an initial concentration of 100 mg L^{-1}, a natural pH of 6.8 (without adjustment), and a contact time of 24 h. Results (Figure 6) show that for all biochars, the AMX removal yields increase with the increase of the adsorbent dose. Indeed, for a small dose of 0.1 g L^{-1}, the AMX removal yields were assessed to be only 3.7%, 6.4%, and 11.3% for Ca-B-700, Ca-B-800, and Ca-B-900, respectively. These yields gradually increase with the increase of the dose to reach quasi-constant performances, with the highest removal yields evaluated to be 68.6%, 86.7%, and 94.7% for Ca-B-700, Ca-B-800, and Ca-B-900, respectively. This behavior is due to the presence of more active adsorption sites for increased doses that can react with AMX molecules. In addition, as specified above, owing to its better physicochemical properties, the Ca-B-900 exhibits the highest AMX removal yield for the lowest required dose (10 g L^{-1}) to reach the performance plateau. For Ca-B-700, a much higher dose (30–40 g L^{-1}) is needed to reach this state (Figure 6). Similar trends were observed in numerous previous studies dealing with AMX removal by engineered biochars [34,46,54].

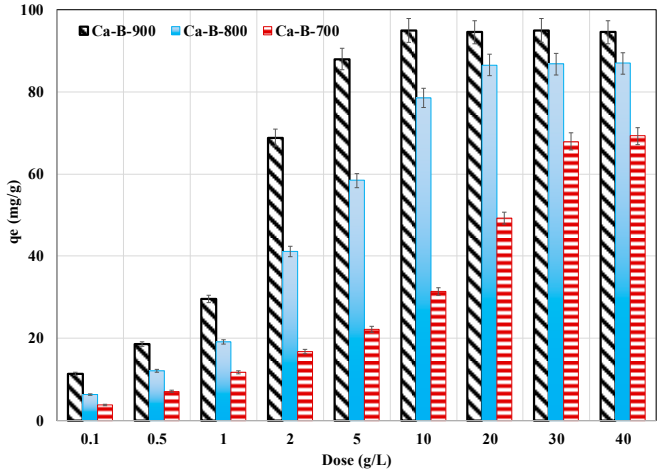

Figure 6. Effect of the tested biochars dose on AMX removal from aqueous solutions.

3.2.4. Impact of Ionic Strength

Since actual wastewater usually contains various ions at different contents, we studied the effect of the presence of dissolved NaCl and Na_2SO_4 on AMX removal for an initial AMX concentration of 100 mg L^{-1}, a non-adjusted pH, and a contact time of 24 h. Results (Figure 7a,b) show that adding Na_2SO_4 at concentrations varying between 1 and 5.2 mM significantly increased the AMX removed amounts (Figure 7a). The largest increase was observed for the highest Na_2SO_4 concentration of 5.2 mM and was evaluated to be 4.1%, 22.3%, and 11.1% for Ca-B-700, Ca-B-800, and Ca-B-900, respectively (Figure 7a). A similar trend was also observed when adding NaCl at concentrations in the range of 14–42 mM. The highest increase of AMX removed amount (30.8%) was observed for Ca-B-900 for a NaCl concentration of 42 mM (Figure 7b). This result indicates that the presence of Na^+ and Cl^- has favored the adsorption of AMX by the synthesized Ca-rich biochars. This finding can be attributed to an improvement in the activity coefficient of AMX [58]. This leads to a decline of AMX solubility and, therefore, can favor its adsorption by the Ca-rich biochars. A comparable trend was reported by Varela et al. [51] when exploring AMX removal by a Zn-modified biochar. These authors reported that increasing NaCl contents from 0.0 to 0.1 M raised the AMX removed amount by 14.9%. Contrarily, other previous studies have shown that an important increase in the ionic strength may result in a non-negligible decrease in AMX removal capacity [59,60].

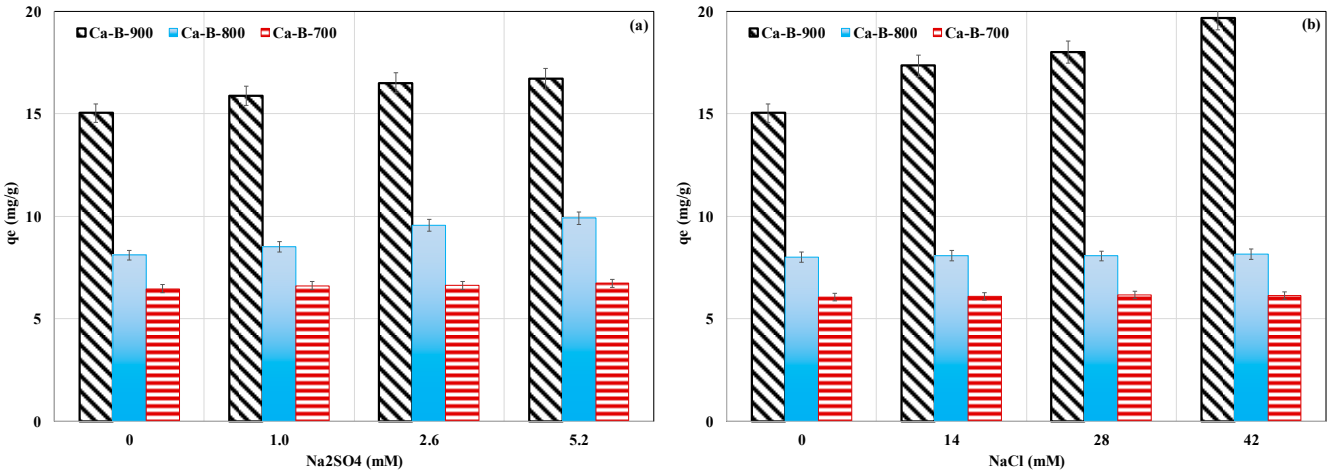

Figure 7. Effect of the presence of Na_2SO_4 (**a**) and NaCl (**b**) on AMX removal by the tested Ca-rich biochars.

3.2.5. Impact of Initial Concentration—Isotherm Study

The effect of the AMX initial concentration on its removal efficiency by the three synthesized biochars is given in Figure 8. It clearly shows that the AMX adsorbed amounts increase when the initial concentration is raised. The highest AMX removed amounts were observed for an initial concentration of 100 mg L^{-1} and were assessed to 8.9, 15.5, and 27.8 mg g^{-1} for Ca-B-700, Ca-B-800, and Ca-B-900, respectively (Figure 8). This is attributed to the fact that higher AMX initial concentrations result in larger concentration gradients between the aqueous and solid media and consequently greater diffusion fluxes in the biochars porosity and, thus, more chances for AMX to be removed [46]. The results of the experimental data fitting to Langmuir, Freundlich, and D-R results are displayed in Figure 8 and Table 4. For Ca-B-700 and Ca-B-800, the D-R and Langmuir models fit the best to the experimental data since the corresponding R^2 and MAPE are respectively higher and lower than those observed for the Freundlich model (Table 4). This suggests that the adsorption of AMX molecules occurs on a monolayer at the surface of these adsorbents with the presence of a finite number of energetically equivalent adsorption sites [49,53,54]. Regarding the Ca-B-900, the Freundlich model is the most suitable, with the highest R^2 (0.962) and the lowest MAPE (7.9%) (Table 4). This indicates that AMX adsorption onto

this adsorbent occurs heterogeneously and on multilayers [61,62]. In addition, for the three biochars, the AMX adsorption is favorable since all the calculated Langmuir's constants ($R_L = \frac{1}{1 + K_{L*C_0}}$) were lower than 1, and the Freundlich coefficient (n) is higher than 1 (Table 4). The Langmuir's adsorption capacities of AMX onto Ca-B-700, Ca-B-800, and Ca-B-900 were assessed to be 13.6, 46.8, and 56.2 mg g^{-1}. The increase of this parameter with the rising pyrolysis temperature is mainly ascribed to the enhancement of the textural properties of the biochars. For instance, the BET surface area of the Ca-B-900 was evaluated to be 14.1 and 3.1 times higher than those of Ca-B-700 and Ca-B-800 (see Table 2).

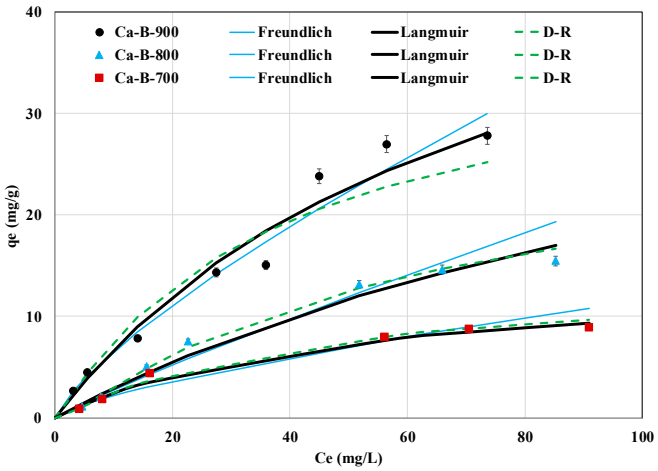

Figure 8. Isotherm experimental data of AMX removal by the synthesized Ca-rich biochars and their fitting with Freundlich, Langmuir, and D-R models.

Table 4. Calculated isotherms parameters for AMX removal by the synthesized Ca-rich biochars.

Isotherm	Parameter	Ca-B-700	Ca-B-800	Ca-B-900
Langmuir	K_L (L mg^{-1})	0.019	0.007	0.0136
	$q_{m,L,pred}$ (mg g^{-1})	14.6	46.8	56.2
	R^2	0.982	0.975	0.962
	MAPE (%)	9.8	12.1	11.4
Freundlich	n	1.38	1.10	1.31
	K_F	0.409	0.346	1.134
	R^2	0.941	0.947	0.962
	MAPE (%)	13.7	14.8	7.9
D-R	$q_{m,D-R,pred}$ (mg g^{-1})	13.6	26.3	37.1
	E (kJ mol^{-1})	4.75	4.24	4.96
	R^2	0.986	0.998	0.941
	MAPE (%)	6.0	4.3	13.8

It is important to underline that the adsorption capacity of Ca-B-900 is about 1.8 and 1.5 times larger than those given for biochars produced from the pyrolysis of Zn-modified sludge [34] and olive stone waste [63] (Table 5). It is comparable to the efficiency of a H_3PO_4-modified biochar from waste coffee grounds [61]. However, the Ca-B-900 efficiency is much lower than biochars derived from the pyrolysis of KOH-modified sludge: 204.0 mg g^{-1} [64], a KOH-pretreated sludge: 305.0 mg g^{-1} [65], and NaOH-pretreated guava seeds: 570.5 mg g^{-1} [66] (Table 5). These latter materials have more interesting physico-chemical properties than our Ca-rich biochars. For instance, the synthesized

NaOH-guava seeds-derived biochar has exceptionally high BET surface area and total pore volume of 2573.6 m^2 g^{-1} and 1.26 cm^3 g^{-1} [66].

Table 5. Comparison of AMX removal capacity of the Ca-rich biochars with other engineered biochars (T: pyrolysis temperature; G: heating gradient; t: residence time; RT: room temperature; -: not given).

Feedstock, Provenance	Pretreatment	Pyrolysis Conditions	Post-Treatment	Adsorption Experimental Conditions	Langmuir's Adsorption Capacity (mg g^{-1})	Reference
Vine wood, Iran	-	T = 600 °C; G = -; t = 2 h	Impregnation with NaOH at a mass ratio of 5%	C_0 = 20–200 mg L^{-1}; pH = 2; D = 0.4 g L^{-1}; t = 8 h; T = 25 °C	2.7	[67]
Industrial sludge, Oman	-	T = 750 °C; G = 5 °C min^{-1}; t = 2 h	-	C_0 = 20–120 mg L^{-1}; pH = 6.8 ; D = 1 g L^{-1}; t = 3 h; T = RT	22.6	[34]
	Impregnation with 1 M $ZnCl_2$				31.9	
	Impregnation with 1 M $FeCl_3$				32.1	
Olive stone, Tunisia	Impregnation with phosphoric acid (50%, by weight) at 110 °C for 9 h	T = 170 °C; G = -; t = 0.5 h, then T = 380 °C; G = -; t = 2.5 h	-	C_0 = 12.5–100 mg L^{-1}; pH = not adjusted; D = 1 g L^{-1}; t = 10 h; T = 20 °C	38.7	[63]
Coffee grounds, South Korea	Impregnation with phosphoric acid at 110 °C for 36 h	T = 600 °C; G = -; t = 2 h	-	C_0 = 0–200 mg L^{-1}; pH = not adjusted; D = 1 g L^{-1}; t = 24 h; T = RT	54.6	[61]
Paper mill sludge, Portugal	Impregnation with KOH at a ratio (KOH/sludge) of 1:5 (*w*/*w*), then sonication for 1 h in an ultrasonic batch	T = 800 °C; G = 15 °C min^{-1}; t = 20 min	-	C_0 = 0–5 mg/L; pH = not adjusted; D = 15 mg L^{-1}; t = 15 h; T = 25 °C	204.0	[64]
Pulp and paper mill sludge, Sweeden	Impregnation with KOH at a mass ratio of 1:1	T = 800 °C; G = 10 °C min^{-1}; t = 3 h	-	C_0 = 0–1000 mg L^{-1}; pH = 6; D = 1.5 g L^{-1}; t = 4 h; T = 25 °C	305.0	[65]
Guava seeds, Brazil	-	T= 500 °C; G = 20 °C min^{-1}; t = 2 h	Impregnation with NaOH at a mass ratio of 3:1 (NaOH/biomass), then pyrolysis for: T= 750 °C; G = - °C min^{-1}; t = 1.5 h	C_0 = 50–800 mg L^{-1}; pH = 4; D = 1 g L^{-1}; t = 4 h; T = 25 °C	570.5	[66]
Mixture of poultry manure and date palm waste, Oman	Mixing with waste marble powder	T = 700 °C; G = 5 °C min^{-1}; t = 2 h	-	C_0 = 5–100 mg L^{-1}; pH = 6.8 ; D = 1 g L^{-1}; t = 20 h; T = RT	14.6	This study
		T = 800 °C; Idem.			46.8	
		T = 900 °C; Idem.			56.2	

Additionally, for all tested biochars, the calculated free energy (E) by the D-R model is lower than 8 kJ mol^{-1} (Table 4), suggesting that AMX adsorption would also involve physical processes [66]. This result is in agreement with that presented by Meghani et al. [46] and Varela et al. [51] regarding AMX removal by biochars derived from ginger waste and corn cobs, respectively.

The main mechanisms involved in AMX removal by the Ca-rich biochars were explored by combining the experimental results (pH effect), the numerical studies (both kinetic and isotherm), and previously published data. Indeed, on the basis of the pH effect and the kinetic and isotherm studies, it seems that the AMX adsorption by the synthe-

sized biochars involves both physical and chemical processes. The physical mechanisms may include low-energy interactions such as pore filling, Van Der Waals, and hydrogen bonds [36]. The chemical processes may encompass electrostatic interactions between the positively charged biochars' particles and the negative forms of AMX (above the pKa_1 of 2.7). Moreover, according to FTIR spectra of the biochars before and after AMX adsorption, only the hydroxyl groups might be involved in the adsorption process. Indeed, for all biochars, the –OH, the narrow peak observed at 3643 cm^{-1} (see Figure 3), has completely disappeared for the three biochars. Moreover, the second O-H peak observed before the adsorption at 3427 cm^{-1} was shifted by +6, +5, and +20 cm^{-1} for Ca-B-700, Ca-B-800, and Ca-B-900, respectively. Besides that, AMX adsorption could also involve π-π interactions between π electrons existing in the aromatic rings of the biochars, the conjugated aromatic rings of AMX [68].

3.3. Challenges and Opportunities

This study shows that Ca-rich biochar may be considered an interesting material for AMX removal from aqueous solutions under static conditions. The precise assessment of AMX and other pharmaceuticals removal for wider experimental conditions under dynamic mode (columns and reactors) is crucial for future work. These dynamic assays have the main advantages of using large-scale plants where the pollutant can be continuously injected through the adsorbent bed in column mode, and either the adsorbate or the adsorbent can be continuously fed to the CSTR system. Such a study should be compared with the related rare previous works [29,31]. Moreover, the management of the pharmaceutical-loaded biochars is another challenge to be ascertained. Nowadays, various chemical reagents have been tested for the effective regeneration of AMX-loaded biochars. They showed that the regenerated biochars could be used for several cycles without a significant decrease in their adsorption capacities [10,69]. The desorbed and concentrated solutions with AMX can be treated by using advanced oxidation processes [70]. Therefore, the optimization of the desorption process and the treatment of the desorbed solution by adapted technologies (i.e., advanced oxidation processes) have to be intensively investigated in the future. Besides these technical challenges, the economic side has to be seriously considered. In this context, the energy consumption during the pyrolysis process should be absolutely reduced. Moreover, important work has to be undertaken regarding the social perception constraints of biochar production and use. Finally, policy challenges concerning solid waste conversion into biochars and their use for wastewater treatment have to be accounted for [71]. In this regard, the implementation of biochar use specific incentives for concerned end users' encouragement could significantly contribute to its widespread application.

Nevertheless, biochar production and use is currently gaining high worldwide attention [15]. According to the latest report of the International Biochar Initiative (IBI), more than 350,000 metric tons of biochar were produced in 2023, and a 91% compound annual growth (CAGR) was estimated for 2021 [72]. Moreover, it is projected that by 2025, biochar revenues will grow further to around USD 3.3 billion [72]. Biochar is usually presented as an interesting alternative to activated carbons (for wastewater treatment) and synthetic fertilizers (for agricultural soil amendment). In our case, the Ca-rich biochars production and use for pharmaceuticals removal and nutrient recovery present remarkable advantages, including (i) better management of huge amounts of poultry manure and date palm waste, as well as industrial marble waste, (ii) preservation of surface water against pollution and eutrophication due to the presence of high contents of nutrients and also pharmaceuticals, (iii) greenhouse gases emission reduction, and (iv) promotion of sustainability and circular economy concepts that is highly recommended by international initiatives such as the United Nations Sustainable Development Goals and also specific future national visions in several countries.

4. Conclusions

This paper demonstrates that Ca-rich biochars generated from the co-pyrolysis of poultry manure, date palm fronds, and waste marble powder can be considered promising materials for amoxicillin removal under wide experimental conditions in batch mode. High AMX removal ability can be obtained through the increase of the pyrolysis temperature, which significantly improves the biochars' structural, textural, and surface chemical properties. The highest AMX removal capacity was observed for Ca-B-900 (56.2 mg g^{-1}), which is relatively high in comparison with some other engineered biochars. The experimental and modeling study shows that the AMX removal process may involve both physical and chemical mechanisms, such as pore filling, π-π interactions, Van Der Waals and hydrogen bonds, electrostatic interactions, and complexation with hydroxyl groups. Further dynamic investigations using laboratory columns and/or reactors are needed in order to confirm these results. Moreover, the management of the AMX-loaded biochars should be explored in the future.

Supplementary Materials: The following supporting information can be downloaded at: https://www.mdpi.com/article/10.3390/pr12081552/s1, Figure S1: SEM/EDS analyses of Ca-B-700 (a), Ca-B-800 (b), and Ca-B-900 (c); Table S1: Kinetic and isotherm model equations used for the fitting of experimental data.

Author Contributions: Conceptualization, S.J., M.A.-H., J.A.-S. and M.J.; methodology, S.J., M.A.-H., J.A.-S., A.A.-R. and M.J.; software, S.J. and W.H.; validation, S.J., W.H. and M.J.; formal analysis, S.J. and W.H.; investigation, M.A.-H., H.A.-N. and A.A.-R.; resources, S.J. and M.A.-W.; data curation, S.J. and W.H.; writing—original draft preparation, S.J. and W.H.; writing—review and editing, W.H., M.A.-W., J.A.-S. and M.J.; visualization, S.J., M.A.-W., H.A.-N. and A.A.-R.; supervision, S.J. and J.A.-S.; project administration, S.J.; funding acquisition, S.J. All authors have read and agreed to the published version of the manuscript.

Funding: This research was funded by Sultan Qaboos University, grant number CL/SQU/QU/CESR/23/01.

Data Availability Statement: Data may be available on request.

Acknowledgments: The authors would like to thank Ibrahim Al-Khusaibi from CAARU for his valuable help on XRD analyses.

Conflicts of Interest: The authors declare no conflicts of interest.

References

1. Yu, Y.; Wang, S.; Yu, P.; Wang, D.; Hu, B.; Zheng, P.; Zhang, M. A bibliometric analysis of emerging contaminants (ECs) (2001–2021): Evolution of hotspots and research trends. *Sci. Total Environ.* **2024**, *907*, 168116. [CrossRef] [PubMed]
2. Omeka, M.E.; Ezugwu, A.L.; Agbasi, J.C.; Egbueri, J.C.; Abugu, H.O.; Aralu, C.C.; Ucheana, I.A. A review of the status, challenges, trends, and prospects of groundwater quality assessment in Nigeria: An evidence-based meta-analysis approach. *Environ. Sci. Pollut. Res.* **2024**, *31*, 22284–22307. [CrossRef] [PubMed]
3. Wang, F.; Xiang, L.; Sze-Yin Leung, K.; Elsner, M.; Zhang, Y.; Guo, Y.; Pan, B.; Sun, H.; An, T.; Ying, G.; et al. Emerging contaminants: A One Health perspective. *Innovation* **2024**, *5*, 100612. [CrossRef] [PubMed]
4. Sumpter, J.P.; Johnson, A.C.; Runnalls, T.J. Pharmaceuticals in the Aquatic Environment: No Answers Yet to the Major Questions. *Environ. Toxicol. Chem.* **2024**, *43*, 589–594. [CrossRef]
5. Rathi, B.S.; Kumar, P.S.; Show, P.L. A review on effective removal of emerging contaminants from aquatic systems: Current trends and scope for further research. *J. Hazard. Mater.* **2021**, *409*, 124413. [CrossRef] [PubMed]
6. Litskas, V.D.; Karamanlis, X.N.; Prousali, S.P.; Koveos, D.S. Effects of the Antibiotic Amoxicillin on Key Species of the Terrestrial Environment. *Bull. Environ. Contam. Toxicol.* **2018**, *100*, 509–515. [CrossRef] [PubMed]
7. Kovalakova, P.; Cizmas, L.; McDonald, T.J.; Marsalek, B.; Feng, M.; Sharma, V.K. Occurrence and toxicity of antibiotics in the aquatic environment: A review. *Chemosphere* **2020**, *251*, 126351. [CrossRef]
8. Nasir, A.; Saleh, M.; Aminzai, M.T.; Alary, R.; Dizge, N.; Yabalak, E. Adverse effects of veterinary drugs, removal processes and mechanisms: A review. *J. Environ. Chem. Eng.* **2024**, *12*, 111880. [CrossRef]
9. Akintola, A.T.; Ayankunle, A.Y. Improving Pharmaceuticals Removal at Wastewater Treatment Plants Using Biochar: A Review. *Waste Biomass Valorization* **2023**, *14*, 2433–2458. [CrossRef]
10. Hama Aziz, K.H.; Mustafa, F.S.; Hassan, M.A.; Omer, K.M.; Hama, S. Biochar as green adsorbents for pharmaceutical pollution in aquatic environments: A review. *Desalination* **2024**, *583*, 117725. [CrossRef]

11. Homem, V.; Alves, A.; Santos, L. Amoxicillin removal from aqueous matrices by sorption with almond shell ashes. *Int. J. Environ. Anal. Chem.* **2010**, *90*, 1063–1084. [CrossRef]
12. Mansour, F.; Al-Hindi, M.; Yahfoufi, R.; Ayoub, G.M.; Ahmad, M.N. The use of activated carbon for the removal of pharmaceuticals from aqueous solutions: A review. *Rev. Environ. Sci. Biotechnol.* **2018**, *17*, 109–145. [CrossRef]
13. Du, C.; Zhang, Z.; Yu, G.; Wu, H.; Chen, H.; Zhou, L.; Zhang, Y.; Su, Y.; Tan, S.; Yang, L.; et al. A review of metal organic framework (MOFs)-based materials for antibiotics removal via adsorption and photocatalysis. *Chemosphere* **2021**, *272*, 129501. [CrossRef]
14. Yu, S.; Zhang, W.; Dong, X.; Wang, F.; Yang, W.; Liu, C.; Chen, D. A review on recent advances of biochar from agricultural and forestry wastes: Preparation, modification and applications in wastewater treatment. *J. Environ. Chem. Eng.* **2024**, *12*, 111638. [CrossRef]
15. Prochnow, F.D.; Cavali, M.; Dresch, A.P.; Belli, I.M.; Libardi, N.J.; de Castilhos, A.B.J. Biochar: From Laboratory to Industry Scale-An Overview Brazilian Context, and Contributions to Sustainable Development. *Processes* **2024**, *12*, 1006. [CrossRef]
16. Samaraweera, H.; Palansooriya, K.N.; Dissanayaka, P.D.; Khan, A.H.; Sillanpää, M.; Mlsna, T. Sustainable phosphate removal using Mg/Ca-modified biochar hybrids: Current trends and future outlooks. *Case Stud. Chem. Environ. Eng.* **2023**, *8*, 100528. [CrossRef]
17. Jellali, S.; Hadroug, S.; Al-Wardy, M.; Al-Nadabi, H.; Nassr, N.; Jeguirim, M. Recent developments in metallic-nanoparticles-loaded biochars synthesis and use for phosphorus recovery from aqueous solutions. A critical review. *J. Environ. Manag.* **2023**, *342*, 118307. [CrossRef] [PubMed]
18. Jellali, S.; Khiari, B.; Al-balushi, M.; Al-sabahi, J.; Hamdi, H.; Bengharez, Z.; Al-abri, M.; Al-nadabi, H.; Jeguirim, M. Use of waste marble powder for the synthesis of novel calcium-rich biochar: Characterization and application for phosphorus recovery in continuous stirring tank reactors. *J. Environ. Manag.* **2024**, *351*, 119926. [CrossRef]
19. Xu, C.; Liu, R.; Chen, L. Removal of Phosphorus from Domestic Sewage in Rural Areas Using Oyster Shell-Modified Agricultural Waste–Rice Husk Biochar. *Processes* **2023**, *11*, 2577. [CrossRef]
20. Xu, Z.C.; Zhang, B.; Wang, T.; Liu, J.; Mei, M.; Chen, S.; Li, J. Environmentally friendly crab shell waste preparation of magnetic biochar for selective phosphate adsorption: Mechanisms and characterization. *J. Mol. Liq.* **2023**, *385*, 122436. [CrossRef]
21. Li, S.; Wang, N.; Chen, S.; Sun, Y.; Li, P.; Tan, J.; Jiang, X. Enhanced soil P immobilization and microbial biomass P by application of biochar modified with eggshell. *J. Environ. Manag.* **2023**, *345*, 118568. [CrossRef] [PubMed]
22. Li, J.; Li, B.; Huang, H.; Lv, X.; Zhao, N.; Guo, G.; Zhang, D. Removal of phosphate from aqueous solution by dolomite-modified biochar derived from urban dewatered sewage sludge. *Sci. Total Environ.* **2019**, *687*, 460–469. [CrossRef] [PubMed]
23. Wang, K.; Peng, N.; Zhang, D.; Zhou, H.; Gu, J.; Huang, J.; Liu, C.; Chen, Y.; Liu, Y.; Sun, J. Efficient removal of methylene blue using $Ca(OH)_2$ modified biochar derived from rice straw. *Environ. Technol. Innov.* **2023**, *31*, 103145. [CrossRef]
24. Wang, L.; Wang, J.; Wei, Y. Facile synthesis of eggshell biochar beads for superior aqueous phosphate adsorption with potential urine P-recovery. *Colloids Surfaces A Physicochem. Eng. Asp.* **2021**, *622*, 126589. [CrossRef]
25. Liao, Y.; Chen, S.; Zheng, Q.; Huang, B.; Zhang, J.; Fu, H.; Gao, H. Removal and recovery of phosphorus from solution by bifunctional biochar. *Inorg. Chem. Commun.* **2022**, *139*, 109341. [CrossRef]
26. Cao, L.; Ouyang, Z.; Chen, T.; Huang, H.; Zhang, M.; Tai, Z.; Long, K.; Sun, C.; Wang, B. Phosphate removal from aqueous solution using calcium-rich biochar prepared by the pyrolysis of crab shells. *Environ. Sci. Pollut. Res.* **2022**, *29*, 89570–89584. [CrossRef] [PubMed]
27. Yang, F.; Chen, Y.; Nan, H.; Pei, L.; Huang, Y.; Cao, X.; Xu, X.; Zhao, L. Metal chloride-loaded biochar for phosphorus recovery: Noteworthy roles of inherent minerals in precursor. *Chemosphere* **2021**, *266*, 128991. [CrossRef] [PubMed]
28. Santos, A.F.; Lopes, D.V.; Alvarenga, P.; Gando-Ferreira, L.M.; Quina, M.J. Phosphorus removal from urban wastewater through adsorption using biogenic calcium carbonate. *J. Environ. Manag.* **2024**, *351*, 119875. [CrossRef] [PubMed]
29. Zeng, S.; Kan, E. Sustainable use of $Ca(OH)_2$ modified biochar for phosphorus recovery and tetracycline removal from water. *Sci. Total Environ.* **2022**, *839*, 156159. [CrossRef]
30. Jin, X.; Guo, J.; Hossain, M.F.; Lu, J.; Lu, Q.; Zhou, Y.; Zhou, Y. Recent advances in the removal and recovery of phosphorus from aqueous solution by metal-based adsorbents: A review. *Resour. Conserv. Recycl.* **2024**, *204*, 107464. [CrossRef]
31. Jellali, S.; Khiari, B.; Al-balushi, M.; Al-harrasi, M.; Al-sabahi, J. Novel calcium-rich biochar synthesis and application for phosphorus and amoxicillin removal from synthetic and urban wastewater: Batch, columns, and continuous stirring tank reactors investigations. *J. Water Process Eng.* **2024**, *58*, 104818. [CrossRef]
32. Shin, J.; Kwak, J.; Son, C.; Kim, S.; Lee, Y.-G.; Kim, H.-J.; Rho, H.; Lee, S.-H.; Park, Y.; Hwa Cho, K.; et al. Oyster shell-doped ground coffee waste biochars for selective removal of phosphate and nitrate ions from aqueous phases via enhanced electrostatic surface complexations: A mechanism study. *J. Environ. Chem. Eng.* **2024**, *12*, 112154. [CrossRef]
33. Jellali, S.; Azzaz, A.A.; Jeguirim, M.; Hamdi, H.; Mlayah, A. Use of lignite as a low-cost material for cadmium and copper removal from aqueous solutions: Assessment of adsorption characteristics and exploration of involved mechanisms. *Water* **2021**, *13*, 164. [CrossRef]
34. Jellali, S.; Khiari, B.; Al-Harrasi, M.; Charabi, Y.; Al-Sabahi, J.; Al-Abri, M.; Usman, M.; Al-Raeesi, A.; Jeguirim, M. Industrial sludge conversion into biochar and reuse in the context of circular economy: Impact of pre-modification processes on pharmaceuticals removal from aqueous solutions. *Sustain. Chem. Pharm.* **2023**, *33*, 101114. [CrossRef]

35. Altıkat, A.; Alma, M.H.; Altıkat, A.; Bilgili, M.E.; Altıkat, S. A Comprehensive Study of Biochar Yield and Quality Concerning Pyrolysis Conditions: A Multifaceted Approach. *Sustainability* **2024**, *16*, 937. [CrossRef]
36. Jellali, S.; Khiari, B.; Usman, M.; Hamdi, H.; Charabi, Y.; Jeguirim, M. Sludge-derived biochars: A review on the influence of synthesis conditions on pollutants removal efficiency from wastewaters. *Renew. Sustain. Energy Rev.* **2021**, *144*, 111068. [CrossRef]
37. Tomczyk, A.; Sokołowska, Z.; Boguta, P. Biochar physicochemical properties: Pyrolysis temperature and feedstock kind effects. *Rev. Environ. Sci. Biotechnol.* **2020**, *19*, 191–215. [CrossRef]
38. Sutcu, M.; Alptekin, H.; Erdogmus, E.; Er, Y.; Gencel, O. Characteristics of fired clay bricks with waste marble powder addition as building materials. *Constr. Build. Mater.* **2015**, *82*, 1–8. [CrossRef]
39. Kwon, E.E.; Lee, T.; Ok, Y.S.; Tsang, D.C.W.; Park, C.; Lee, J. Effects of calcium carbonate on pyrolysis of sewage sludge. *Energy* **2018**, *153*, 726–731. [CrossRef]
40. Deng, W.; Zhang, D.; Zheng, X.; Ye, X.; Niu, X.; Lin, Z.; Fu, M.; Zhou, S. Adsorption recovery of phosphate from waste streams by Ca/Mg-biochar synthesis from marble waste, calcium-rich sepiolite and bagasse. *J. Clean. Prod.* **2021**, *288*, 125638. [CrossRef]
41. Liu, Y.; Wang, S.; Huo, J.; Zhang, X.; Wen, H.T.; Zhang, D.; Zhao, Y.; Kang, D.; Guo, W.; Ngo, H.H. Adsorption recovery of phosphorus in contaminated water by calcium modified biochar derived from spent coffee grounds. *Sci. Total Environ.* **2024**, *909*, 168426. [CrossRef] [PubMed]
42. Liu, X.; Lv, J. Efficient Phosphate Removal from Wastewater by Ca-Laden Biochar Composites Prepared from Eggshell and Peanut Shells: A Comparison of Methods. *Sustainability* **2023**, *15*, 1778. [CrossRef]
43. Xu, Y.; Liao, H.; Zhang, J.; Lu, H.; He, X.; Zhang, Y.; Wu, Z.; Wang, H.; Lu, M. A Novel Ca-Modified Biochar for Efficient Recovery of Phosphorus from Aqueous Solution and Its Application as a Phosphorus Biofertilizer. *Nanomaterials* **2022**, *12*, 2755. [CrossRef] [PubMed]
44. Qin, J.; Zhang, C.; Chen, Z.; Wang, X.; Zhang, Y.; Guo, L. Converting wastes to resource: Utilization of dewatered municipal sludge for calcium-based biochar adsorbent preparation and land application as a fertilizer. *Chemosphere* **2022**, *298*, 134302. [CrossRef] [PubMed]
45. Choi, Y.K.; Jang, H.M.; Kan, E.; Wallace, A.R.; Sun, W. Adsorption of phosphate in water on a novel calcium hydroxide-coated dairy manure-derived biochar. *Environ. Eng. Res.* **2019**, *24*, 434–442. [CrossRef]
46. Meghani, R.; Lahane, V.; Kotian, S.Y.; Lata, S.; Tripathi, S.; Ansari, K.M.; Yadav, A.K. Valorization of Ginger Waste-Derived Biochar for Simultaneous Multiclass Antibiotics Remediation in Aqueous Medium. *ACS Omega* **2023**, *8*, 11065–11075. [CrossRef] [PubMed]
47. Hadroug, S.; Jellali, S.; Jeguirim, M.; Kwapinska, M.; Hamdi, H.; Leahy, J.J.; Kwapinski, W. Static and dynamic investigations on leaching/retention of nutrients from raw poultry manure biochars and amended agricultural soil. *Sustainability* **2021**, *13*, 1212. [CrossRef]
48. Mitrogiannis, D.; Psychoyou, M.; Baziotis, I.; Inglezakis, V.J.; Koukouzas, N.; Tsoukalas, N.; Palles, D.; Kamitsos, E.; Oikonomou, G.; Markou, G. Removal of phosphate from aqueous solutions by adsorption onto $Ca(OH)_2$ treated natural clinoptilolite. *Chem. Eng. J.* **2017**, *320*, 510–522. [CrossRef]
49. Shan, G.N.M.; Rafatullah, M.; Siddiqui, M.R.; Kapoor, R.T.; Qutob, M. Calcium oxide from eggshell wastes for the removal of pharmaceutical emerging contaminant: Synthesis and adsorption studies. *J. Indian Chem. Soc.* **2024**, *101*, 101174. [CrossRef]
50. Jellali, S.; Azzaz, A.A.; Al-Harrasi, M.; Charabi, Y.; Al-Sabahi, J.N.; Al-Raeesi, A.; Usman, M.; Al Nasiri, N.; Al-Abri, M.; Jeguirim, M. Conversion of Industrial Sludge into Activated Biochar for Effective Cationic Dye Removal: Characterization and Adsorption Properties Assessment. *Water* **2022**, *14*, 2206. [CrossRef]
51. Varela, C.F.; Moreno-Aldana, L.C.; Agámez-Pertuz, Y.Y. Adsorption of pharmaceutical pollutants on $ZnCl_2$-activated biochar from corn cob: Efficiency, selectivity and mechanism. *J. Bioresour. Bioprod.* **2024**, *9*, 58–73. [CrossRef]
52. Ma, Y.; Li, P.; Yang, L.; Wu, L.; He, L.; Gao, F.; Qi, X.; Zhang, Z. Iron/zinc and phosphoric acid modified sludge biochar as an efficient adsorbent for fluoroquinolones antibiotics removal. *Ecotoxicol. Environ. Saf.* **2020**, *196*, 110550. [CrossRef] [PubMed]
53. Fan, X.; Qian, Z.; Liu, J.; Geng, N.; Hou, J.; Li, D. Investigation on the adsorption of antibiotics from water by metal loaded sewage sludge biochar. *Water Sci. Technol.* **2021**, *83*, 739–750. [CrossRef] [PubMed]
54. Grimm, A.; Chen, F.; Simões dos Reis, G.; Dinh, V.M.; Khokarale, S.G.; Finell, M.; Mikkola, J.P.; Hultberg, M.; Dotto, G.L.; Xiong, S. Cellulose Fiber Rejects as Raw Material for Integrated Production of *Pleurotus* spp. Mushrooms and Activated Biochar for Removal of Emerging Pollutants from Aqueous Media. *ACS Omega* **2023**, *8*, 5361–5376. [CrossRef] [PubMed]
55. Wang, T.; Jiang, M.; Yu, X.; Niu, N.; Chen, L. Application of lignin adsorbent in wastewater Treatment: A review. *Sep. Purif. Technol.* **2022**, *302*, 122116. [CrossRef]
56. Chakhtouna, H.; Benzeid, H.; Zari, N.; el kacem Qaiss, A.; Bouhfid, R. Functional $CoFe_2O_4$-modified biochar derived from banana pseudostem as an efficient adsorbent for the removal of amoxicillin from water. *Sep. Purif. Technol.* **2021**, *266*, 118592. [CrossRef]
57. Allwar, A.; Herawati, M.; Wardana, F.S.; Khoirunnisa, A.; Anugrah, Z.M. Composite of Ag_2O-CuO/biochar as an adsorbent for removal of amoxicillin and paracetamol from aqueous solution. *Int. J. Environ. Sci. Technol.* **2023**, *20*, 13411–13422. [CrossRef]
58. Zhang, Y.; Zhu, C.; Liu, F.; Yuan, Y.; Wu, H.; Li, A. Effects of ionic strength on removal of toxic pollutants from aqueous media with multifarious adsorbents: A review. *Sci. Total Environ.* **2019**, *646*, 265–279. [CrossRef]
59. Yunusa, U.; Umar, U.; Idris, S.A.; Kubo, A.I.; Abdullahi, T. Experimental and DFT computational insights on the adsorption of selected pharmaceuticals of emerging concern from water systems onto magnetically modified biochar. *J. Turkish Chem. Soc. Sect. A Chem.* **2021**, *8*, 1179–1196. [CrossRef]

60. Wu, Q.; Zhang, Y.; Cui, M.-h.; Liu, H.; Liu, H.; Zheng, Z.; Zheng, W.; Zhang, C.; Wen, D. Pyrolyzing pharmaceutical sludge to biochar as an efficient adsorbent for deep removal of fluoroquinolone antibiotics from pharmaceutical wastewater: Performance and mechanism. *J. Hazard. Mater.* **2022**, *426*, 127798. [CrossRef]
61. Choi, S.W.; Hong, J.; Youn, S.; Kim, I. Removal of amoxicillin by coffee grounds biochar with different pretreatment methods. *Environ. Adv.* **2023**, *14*, 100446. [CrossRef]
62. Herrera, K.; Morales, L.F.; López, J.E.; Montoya-Ruiz, C.; Muñoz, S.; Zapata, D.; Saldarriaga, J.F. Biochar production from tannery waste pyrolysis as a circular economy strategy for the removal of emerging compounds in polluted waters. *Biomass Convers. Biorefinery* **2023**. [CrossRef]
63. Limousy, L.; Ghouma, I.; Ouederni, A.; Jeguirim, M. Amoxicillin removal from aqueous solution using activated carbon prepared by chemical activation of olive stone. *Environ. Sci. Pollut. Res.* **2017**, *24*, 9993–10004. [CrossRef] [PubMed]
64. Sousa, É.; Rocha, L.; Jaria, G.; Gil, M.V.; Otero, M.; Esteves, V.I.; Calisto, V. Optimizing microwave-assisted production of waste-based activated carbons for the removal of antibiotics from water. *Sci. Total Environ.* **2021**, *752*, 141662. [CrossRef] [PubMed]
65. Simões Dos Reis, G.; Bergna, D.; Tuomikoski, S.; Grimm, A.; Lima, E.C.; Thyrel, M.; Skoglund, N.; Lassi, U.; Larsson, S.H. Preparation and Characterization of Pulp and Paper Mill Sludge-Activated Biochars Using Alkaline Activation: A Box-Behnken Design Approach. *ACS Omega* **2022**, *7*, 32620–32630. [CrossRef] [PubMed]
66. Pezoti, O.; Cazetta, A.L.; Bedin, K.C.; Souza, L.S.; Martins, A.C.; Silva, T.L.; Santos Júnior, O.O.; Visentainer, J.V.; Almeida, V.C. NaOH-activated carbon of high surface area produced from guava seeds as a high-efficiency adsorbent for amoxicillin removal: Kinetic, isotherm and thermodynamic studies. *Chem. Eng. J.* **2016**, *288*, 778–788. [CrossRef]
67. Pouretedal, H.R.; Sadegh, N. Effective removal of Amoxicillin, Cephalexin, Tetracycline and Penicillin G from aqueous solutions using activated carbon nanoparticles prepared from vine wood. *J. Water Process Eng.* **2014**, *1*, 64–73. [CrossRef]
68. Tan, X.; Liu, Y.; Zeng, G.; Wang, X.; Hu, X.; Gu, Y.; Yang, Z. Application of biochar for the removal of pollutants from aqueous solutions. *Chemosphere* **2015**, *125*, 70–85. [CrossRef] [PubMed]
69. Krasucka, P.; Pan, B.; Sik Ok, Y.; Mohan, D.; Sarkar, B.; Oleszczuk, P. Engineered biochar—A sustainable solution for the removal of antibiotics from water. *Chem. Eng. J.* **2021**, *405*, 126926. [CrossRef]
70. Azzaz, A.A.; Jellali, S.; Akrout, H.; Assadi, A.A.; Bousselmi, L. Dynamic investigations on cationic dye desorption from chemically modified lignocellulosic material using a low-cost eluent: Dye recovery and anodic oxidation efficiencies of the desorbed solutions. *J. Clean. Prod.* **2018**, *201*, 28–38. [CrossRef]
71. Pathy, A.; Ray, J.; Paramasivan, B. Challenges and opportunities of nutrient recovery from human urine using biochar for fertilizer applications. *J. Clean. Prod.* **2021**, *304*, 127019. [CrossRef]
72. Gray, M.; Smith, L.B.; Maxwell-Barton, W.L. *Global Biochar Market Report*. 2023, pp. 1–30. Available online: https://biochar-international.org/2023-global-biochar-market-report/ (accessed on 2 July 2024).